This project has received funding from the European Union's
Seventh Framework Programme
for research, technological development and demonstration
under grant agreement n. 619326

III-V-MOS

Technology CAD for III-V Semiconductor-based MOSFETs

Project number: 619326

Start date: 01/11/2013

Call (part) identifier: FP7-ICT-2013-11

Funding scheme: Collaborative project

D3.7 – Electron drift velocity and diffusion coefficient dependence on electric field at low driving fields in bulk and on-insulator InGaAs

Nature: **Report**

Dissemination Level: **Public (PU)**

Due date: **M36**

Actual submission date: **01/12/2016 modified 31/07/2017**

Participants involved: **IBM**

Authors: **L. Czornomaz (IBM)**

Edited by: **L. Czornomaz (IBM)**

Approvals

Role	Name	Company	Date
Coordinator	L. Selmi	IUNET	01/12/2016
WP3 Leader	L. Czornomaz	IBM	01/12/2016

Revisions History

Revision	Date	Modification	Reviewed by
V0	27/09/16	Creation of D3.7 document	L. Czornomaz, IBM
V1	21/10/16	First draft	L. Czornomaz, IBM
V2	14/11/16	Reviewed	L. Czornomaz, IBM
V3	30/11/16	Review	L. Selmi, IUNET

Content

Executive summary

The objective of the work presented in this deliverable is to characterize the electron drift velocity and diffusion coefficient versus applied electric field in InGaAs by the time-of-flight technique, in order to support the modelling of fundamental InGaAs properties in WP2 and WP4.

Due to the requirements of this project, the technique was adapted from a vertical “bulk” configuration to a lateral “thin-film” configuration. Dedicated time-of-flight setup was realized, and dedicated devices were designed, fabricated and characterized to study transport in InGaAs-on-insulator samples.

ToF devices were successfully characterized for their DC and time-resolved transient response under illumination of the pulsed laser as a function of the applied bias, laser position and laser power.

The results indicates that the required laser power to measure a sufficient time resolved transient current signal is too high, such that the cloud of electron-hole pairs has a too high density and its internally created electric field screens the externally applied electric field. Therefore, carriers are not separated and drifting through the sample as expected in a ToF experiment. The acquired data has nevertheless been delivered to the modelling partners to study the dynamics of the generation-recombination transients in these devices, and its relation to the density of interface and border traps, which are known to hamper the performance of state-of-the-art III-V MOSFETs.

As regards the originally conceived use of the ToF data for calibration of velocity-field characteristics in thin III-V semiconductor films, a backup strategy has been implemented based on curves calculated with the most advanced high-level tools developed within the project.

Report

1.1. Introduction

This deliverable describes the work done at IBM on deliverable D3.7 “Electron drift velocity and diffusion coefficient dependence on electric field at low driving fields in bulk and on-insulator InGaAs”.

The objective of the work presented in this deliverable is to characterize intrinsic transport properties of InGaAs in order to support the modelling of fundamental InGaAs properties in WP2 and WP4. In particular, the focus was to measure the electron drift velocity and diffusion coefficient versus applied electric field. These data will directly feed into the calibration of Monte-Carlo electron transport models which can later be applied to simulate the channel transport properties of an InGaAs MOSFET.

The measurement principle used to extract drift velocity and diffusion coefficient is the Time-of-flight technique, acknowledge as being the most reliable method to extract those parameters (Canali, 2005). Due to the requirements of this project, the technique was adapted from a vertical “bulk” configuration to a lateral “thin-film” configuration. An experimental setup and its associated control software were developed, a specific maskset and process flow were created, and dedicated wafers were fabricated.

Section 1.2 describes the measurement technique and its implementation in a lateral “thin-film” configuration. Section 1.3 describes the maskset, process flow and sample fabrication. Section 1.4 describes the experimental setup and procedure to realize the time-of-flight measurements. Section 1.5 presents the DC and time-of-flight electrical measurements acquired on the samples.

1.2. Time-of-Flight measurements in a lateral "thin-film" configuration

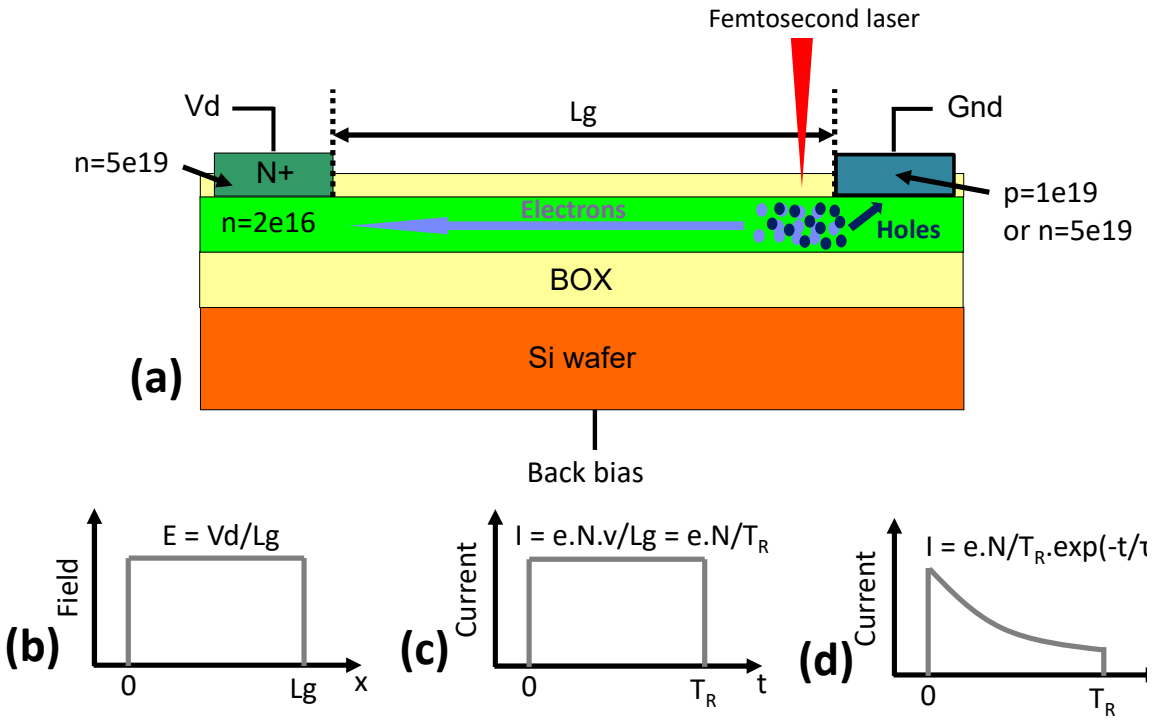

Figure 1: (a) Schematic representation of a time-of-flight measurement applied to an InGaAs-on-insulator thin-film with its contacts. A femto-second laser is applied on the InGaAs-on-insulator thin-film creating electron-hole pairs next to the grounded contact. Under the applied electric-field, electrons and holes are separated. Holes immediately reach the ground contact while electrons drift laterally through the sample over a distance Lg and are collected at the biased (Vd) contact. (b) Schematic representation of the constant electric field (E) across the sample under the assumption of a "minimal perturbation" by the electron-hole pairs. (c) Transient current (I) versus time induced by the density of electrons (N) drifting through the sample at a velocity v for a drift time T_R under the assumption of constant electric-field and no charge trapping. (d) Transient current versus time induced by drifting electrons in the presence of traps with a time constant τ.

The basic idea of the time-of-flight (ToF) technique is to evaluate the transit time taken by charge carriers to travel across a given region of the sample under the influence of a known electric field. In this project, $In_{0.53}Ga_{0.47}As$ thin-films on insulator on Si substrates are investigated. Therefore in this experiment carriers have to travel in-plane, unlike in most ToF

experiments where carriers are traveling vertically in the thickness of a bulk sample. A schematic representation of a ToF measurement applied to an InGaAs-on-insulator thin-film is presented in Fig. 1(a). A pulsed ionizing radiation (a femtosecond laser in our experiment) of sufficient energy to generate electron-hole pairs hits the ground contact of a two-terminal InGaAs-on-insulator device of length Lg. Electron-hole pairs are generated near the ground contact and the presence of a uniform electric-field under the applied bias Vd (Fig. 1(b)) enables electrons to travel across the sample while holes are directly collected at the ground contact. Electrons traveling across the whole Lg region will induce a transient current signal whose duration T_R is the time electron takes to cross the Lg region (Fig. 1(c)). The incoming radiation should have an intensity low enough to avoid space-charge effects and should be short enough so that its pulse duration is small compared to the transit time of carriers across the sample. The area illuminated by the radiation should be small enough compared to the drift region Lg. The carrier lifetime should be longer than the transit time. In the presence of traps with a time constant τ, the transient current is exponentially decaying with time as mobile carriers are getting trapped (Fig. 1(d)). The transit time can still be measured provided that a measurable portion of mobile carriers can still reach the biased contact.

In this experiment, the biased contact consists of highly n-doped InGaAs, while two doping types were evaluated for the ground contact. With a p-doped ground contact, a back-gated PnN junction is formed which can be reverse-biased to produce a uniform electric field in the depletion region. In this configuration, almost no DC current (except for the small dark current) flows in the sample in the absence of the generated electron-hole pairs. With a n-type doped ground contact, a back-gated MOSFET is formed which can be forward biased to to produce a uniform electric field. In this configuration, a constant DC current flows in the device which can be controlled by the back-gate bias. The transient current generated by the electron-holes pairs adds to the DC current.

While both configurations are interesting, simulations showed that given the unintentional n-type background doping of $2x10^{16}$ cm^{-3} in the InGaAs drift layer (see Fig. 1(a)), the extent of the depletion region of the PnN diode is limited to a few microns. The expected maximum drift velocity of electrons is on the order of 10^7 cm/s which would correspond to a transit time of less than 0.5 ns in the reverse-biased PnN diode which is too short to be accurately

measured. Therefore, the experimental work was focused on the back-gated MOSFET configuration with two highly n-doped contacts.

1.3. Fabrication of test structures

A dedicated experimental maskset was designed to realize the ToF test structures. It includes producing dedicated InGaAs-on-insulator on Si wafers with varying InGaAs channel thickness, designing and fabricating a new set of optical masks and developing the corresponding process.

The fabrication of InGaAs-OI wafers (described in Fig. 2(a)) starts with 2" semi-insulating high-grade (100)-oriented InP donor wafers loaded in a MOVPE system. An $In_{0.53}Ga_{0.47}As/In_{0.52}Al_{0.48}As$ etch-stop heterostructure is then grown at 550ºC followed by the growth of the future active layer: an $In_{0.53}Ga_{0.47}As$ channel of varying thickness (25 nm, 50 nm, 100 nm and 200 nm). Subsequently, the wafers are loaded in an Atomic Layer Deposition tool (ALD) where the optimized MOS gate stack (0.5 nm Al_2O_3 / 2 nm HfO_2 described in D3.2) is deposited, followed by 5-nm-thick Al_2O_3.

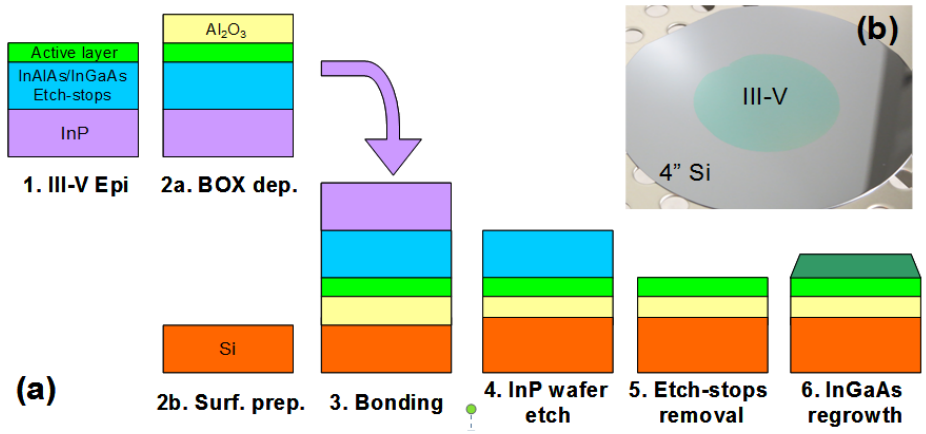

Figure. 2: (a) Schematic process flow of the fabrication of InGaAs-on-insulator substrates (1 to 5) and InGaAs regrowth module for S/D regions (6). (b) Picture of an InGaAs-on-insulator substrate.

The target 4" (100)-oriented p-type (N_A = 2×10^{17} cm^{-3}) Si wafers are wet cleaned for organic contaminants and their native oxide is stripped in diluted hydrofluoric acid (DHF). A thin and

high quality native oxide is then chemically regrown by exposing the wafers to ozone-rich de-ionized water (DIO_3), making their surfaces hydrophilic. Subsequently, a 25-nm-thick SiO_2 grown oxide is thermally and a 5-nm-thick Al_2O_3 is deposited by ALD. The donor and target wafer surfaces are brought into intimate contact at room temperature and ambient atmosphere to initiate the bonding. The wafers are then annealed at 300ºC for 2 hours in order to raise the bonding energy. The InP donor wafers are then etched in concentrated hydrochloric acid until reaching the InGaAs/InAlAs etch-stop heterostructure. This etch-stop structure is finally etched in diluted acids to ensure a soft-landing on the active layer. An example of the resulting InGaAs-OI substrate is shown in Fig. 2(b). The final InGaAs-OI wafers thus have a composition of 53%-Indium, a channel thickness of 25nm, 50nm, 100nm or 200nm, and a buried oxide (BOX) thickness of 25 nm SiO_2 / 10 nm Al_2O_3 and the MOS gate stack (0.5 nm Al_2O_3 / 2 nm HfO_2) resulting in an EOT of 30.6 nm (C_{ox} = 0.11uF/cm^2). The background doping in the channel (n-region) is expected to be n-type around 1-2x10^{16}cm^{-3}.

A set of masks was designed and fabricated. It contains the time-of-flight test structures for this work, and also lateral transport test structures (N+/n/N+) and contact test structures for the deliverable D3.4. Details are given in Fig. 3. It contains in total 8 levels of lithography: alignment marks, N+ regrowth, P+ regrowth (for time-of-flight structures), mesa isolation, metal 1 (M1) contact opening, M1 contacts, M2 contact opening and M2 contacts. Two levels of metals were needed for the time-of-flight structures to minimize parasitic capacitances between the RF-probe pads and the substrate. For the lateral transport test structures, only M1 contacts were used.

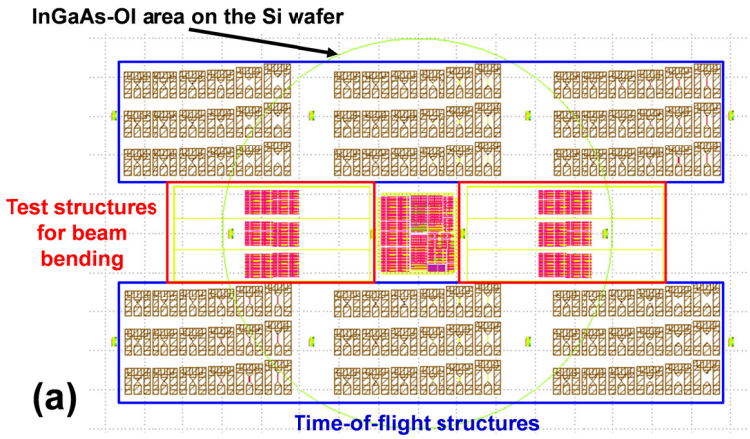

Figure 3: (a) Mask layout overview designed for III-V-MOS. The green circle highlights the 2" InGaAs-OI area of the 4" Si wafer. The blue rectangles indicate the location of the time-of-flight test structures for this deliverable. The red rectangles locate the test structures for D3.4.

A process flow was developed for the joint fabrication ToF test structures as well as for lateral N+/n/N+ test structures for D3.4. Schematics of the fabrication process are shown in Fig. 4. First, a silicon oxide hard mask is deposited on the prepared InGaAs-OI wafers and patterned to block the selective growth of the N+ layer (Fig. 4(a)). The wafers are loaded in the epitaxy chamber, and 50 nm of Sn-doped $In_{0.53}Ga_{0.47}As$ is grown selectively to SiO_2 (Fig. 4(b)). The hard mask is then removed by wet etching (Fig. 4(c)) and a mesa isolation is formed by wet etching the InGaAs down to the BOX (Fig. 4(d)). The optimized MOS gate stack (0.5 nm Al_2O_3 / 2 nm HfO_2 described in D3.2) is deposited followed by a first interlayer dielectric (ILD) consisting of 100 nm SiO_2 (Fig. 4(e)). Contact openings are then formed by dry etching and refilled by W which is later patterned into M1 pads (Fig. 4(f)). A second interlayer dielectric consisting of 2 microns of SiO2 is deposited and patterned to form vias landing on the M1 pads. A 300nm thick gold layer is formed by lift-off, connecting the small M1 pads to large M2 electrodes. Finally, the samples are annealed in H2/Ar ambient to reduce the interface-state density at the various InGaAs/oxide interfaces. The spacing between the two N+ regions is defined by the first SiO_2 hard mask and is later referred as the gate length L_g. Thickness and doping concentration of all the relevant layers are given in Table 1 (Appendix).

It should be noted that there is an optimized MOS gate stack on either side of InGaAs channel in the gate region (towards the BOX at the bottom and the interlayer dielectric on top). This layer is optimized to produce minimum interfacial trap density on top interface of InGaAs. Although those interfaces are nominally the same in terms of the cleaning steps and deposited materials, they differ from the thermal budget to which they were exposed. The bottom interface has been subjected to the thermal budget of the doped selective epitaxy (550°C) while the top interface has only seen the thermal budget of the metal interconnects (< 400°C). In that sense, the bottom interface corresponds to a “gate-first” process while the top interface corresponds to a “replacement-gate” process – referring to D3.8.

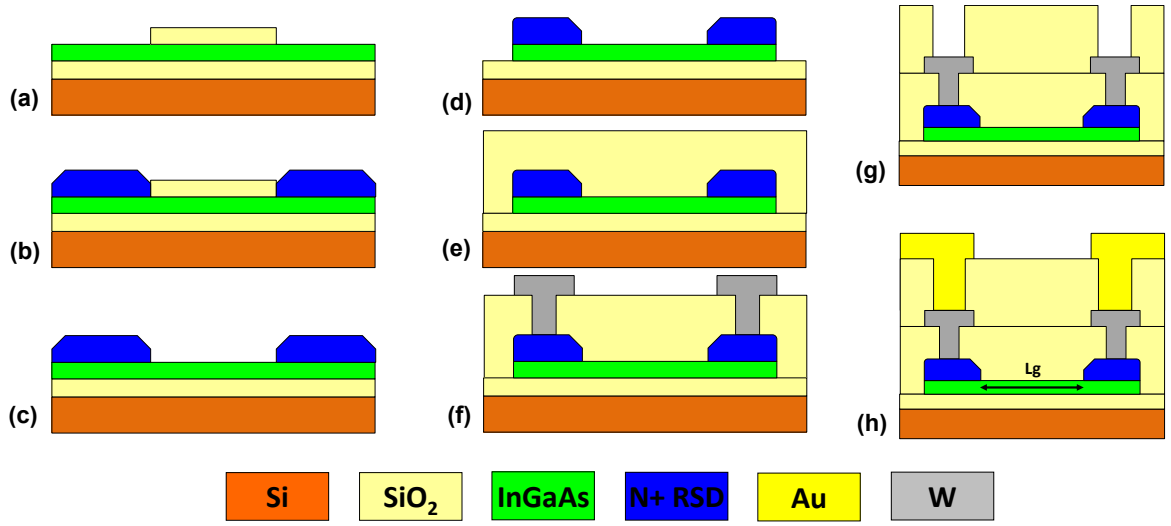

Figure 4: Schematic of the fabrication process for ToF test structures. (a) InGaAs-OI substrate with an SiO2 hard mask, (b) selective epitaxy of N+ InGaAs, (c) removal of SiO2 hard mask, (d) mesa isolation by wet etching, (e) interlayer dielectric deposition (f) contact opening and metal contact definition, (g) second interlayer dielectric and second via opening, (h) gold metallization for lower RF losses..

1.4. Experimental Time-of-Flight setup

In order to perform the time-of-flight measurements, an experimental setup and its associated control software were specially developed for this project (Fig. 5(a)).

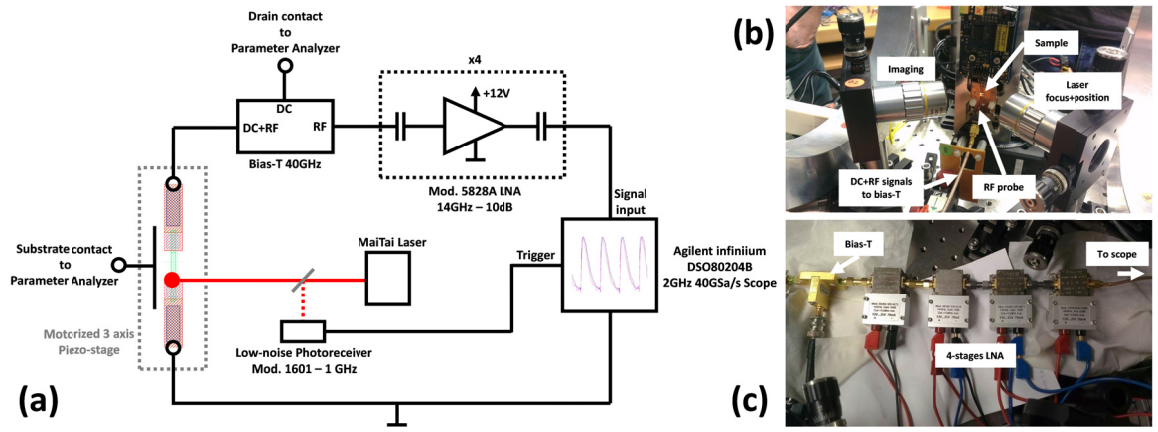

Figure 5: (a) Schematic description of the experimental setup for time-of-flight measurements. (b) Photograph of the setup where the sample is located. It is contacted with an RF picoprobe and pumped with a femtosecond laser through the objective on the right. The objective on the left enables making an image of the sample to accurately position the laser. (c) Photograph of the RF bias-T and RF 4-stage low-noise amplifiers sending the RF signal from the sample to the scope.

First, it consists of a motorized 3-axis piezo-stage on which is mounted the sample (Fig. 5(b)). This stage allows sub-micrometer displacement of the sample for positioning and focusing the laser accurately, but it has no close-loop control so absolute displacements are not reliable. The back-side of the sample is connected with a conductive In-Ga eutectic paste to a copper plate isolated from the ground which can be connected to a parameter analyser in order to apply a bias to the substrate.

Second, an RF picoprobe is used to contact the device in a ground-signal-ground coplanar waveguide configuration. The signal and ground lines are connected to the drain and source of the device, respectively. The RF picoprobe is connected to the DC+RF port of a bias-T with a bandwidth of 40 GHz. A DC bias can be applied to the drain of the device with a parameter analyser connected to the DC port of the bias-T. The RF port of the bias-T (where the transient small RF signal is coupled to) is connected to a 4-stage low-noise amplifier with a 14 GHz bandwidth and a nominal gain of 10 dB per stage (Fig. 5(c)). The amplified transient RF signal is sent to the internal 50 Ω load of an Agilent infiniium DSO80204B fast

oscilloscope, converting the transient current in a transient voltage which can be recorded by the scope.

Third, a tunable femtosecond MaiTai Ti:Sapphire laser from Spectra-Physics is used as an ionization source for the time-of-flight measurements. It produces ≈100 fs laser pulses every 12 ns at a wavelength of 820 nm and with an average power of 150 mW. The laser pulses are monitored with a low-noise photoreceiver with a 1 GHz bandwidth, whose signal is used to trigger the fast oscilloscope. Before reaching the sample, the laser beam can be attenuated with a set of filters, which offer a tuning range of the transmission coefficient of 3 orders of magnitude and in addition, an ON/OFF filter with a 10^{-7} transmission coefficient. As a result, the transmission coefficient can be tuned between 10^{-10} and 10^{-7}, and between 10^{-3} and 1. The laser is focused on the sample with a final spot size of ≈ 2 µm.

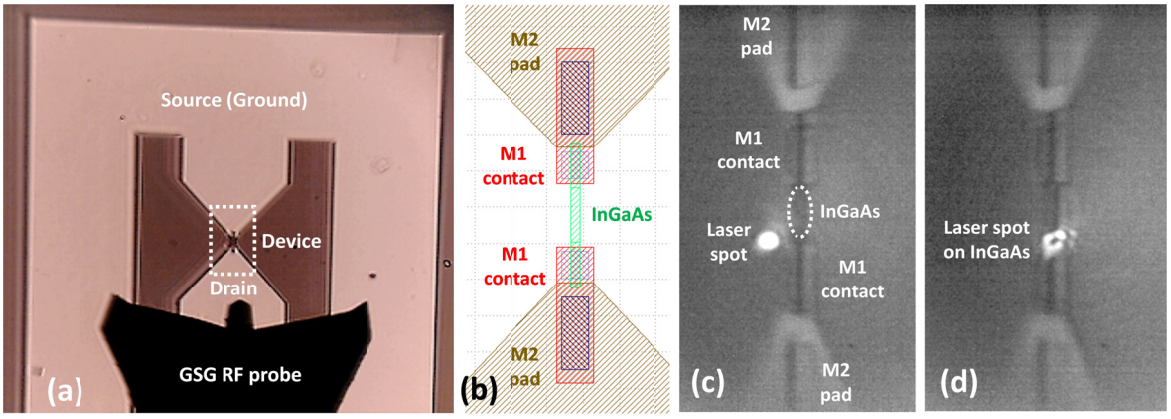

Figure 6: (a) Image of a ToF device under test, contacted by an RF picoprobe in ground-signal-ground configuration. The central signal line is connected to the drain of the device, the side ground lines to the source of the device. (b) Layout of the ToF device with the 2.5 µm-wide InGaAs drift layer (green), the small M1 pads (red) and the M2 pads (brown). (c) Corresponding image of the ToF device under test from (a), observed with the imaging objective. Comparing this image to (b), the InGaAs drift layer, the M1 and M2 pads can be easily recognized. The focused laser spot is also visible, on the left side on the InGaAs drift layer. (d) Same image as (c) but with the laser spot accurately aligned to the edge of the drain M1 contact.

Figure 6(a) presents a top view image of a ToF device under test, connected with the RF picoprobe. The laser can be accurately aligned to the edge of the drain M1 contact (Fig.

6(b,c,d)) by scanning the x- and y- axis of the piezo-stage and recording the peak transient voltage on the scope. First, the laser is centered on the InGaAs drift layer by scanning the sample position from left to right and finding the maximum signal intensity. Then, the sample is moved upwards until the ToF signal disappears indicating that the laser is not hitting the InGaAs drift layer anymore, but rather the M1 contact made of tungsten, which is not transparent at this wavelength. The sample is then moved to the last position before the signal starts to drop (before the laser starts to hit the drain M1 contact). This alignment procedure is later referred as an alignment to the “drain contact edge”. In a similar way, the laser can be aligned to the “source contact edge”.

1.5. DC and Time-of-flight measurements

The approach used for DC electrical characterization is similar to that generally used for pseudo-MOS test structures (see D3.4). In brief, the Si substrate/BOX acts as a back-gate terminal and the N+ InGaAs areas are used as source and drain terminals. The gate length (L_g) is defined as the distance between the N+ InGaAs areas.

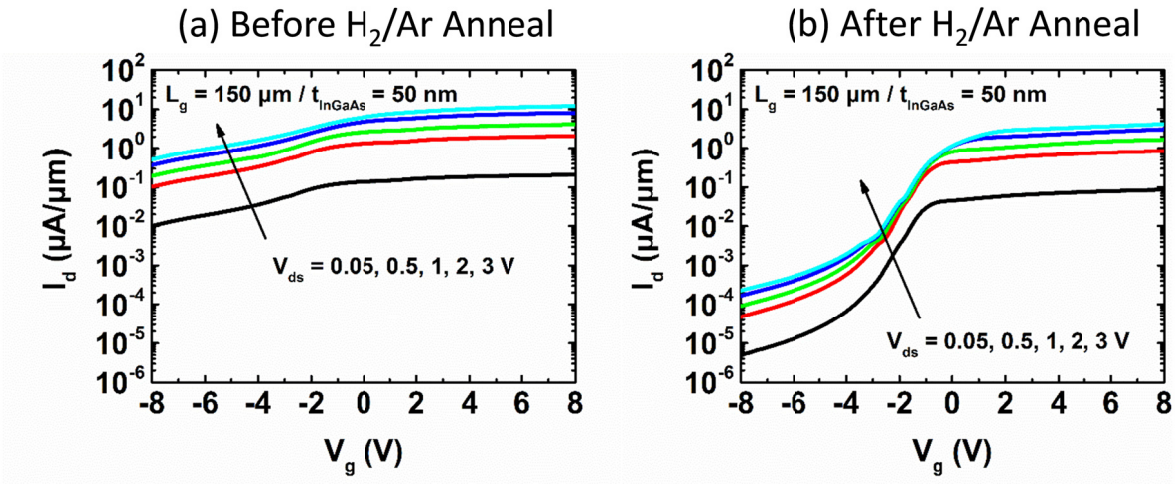

Figure 7: I_d-V_g characteristics measured for V_{ds} = 0.05, 0.5, 1, 2, and 3 V on fabricated ToF test structures featuring L_g = 150 µm and t_{InGaAs} = 50 nm: (a) before H2/Ar anneal – same as in D3.4, (b) after H2/Ar anneal.

Figure 7 presents Id-Vg transfer characteristics acquired the same ToF device with a gate length of 150 µm and an InGaAs drift layer thickness of 50 nm, before and after H2/Ar anneal. Before the annealing step, it is clear that it is very difficult to turn off the transistor as indicated by a low I_{ON}/I_{OFF} ratio of about an order of magnitude. After H2/Ar anneal, the I_{ON}/I_{OFF} ratio improves to above 4 orders of magnitude, indicating that the annealing step improved the gate control over the channel by passivating some of the interface-states at the InGaAs/oxide interface – which is very desirable since mobile carriers should not be trapped during ToF measurements (see section 1.2). All samples studied in this deliverable were subjected to this H2/Ar anneal.

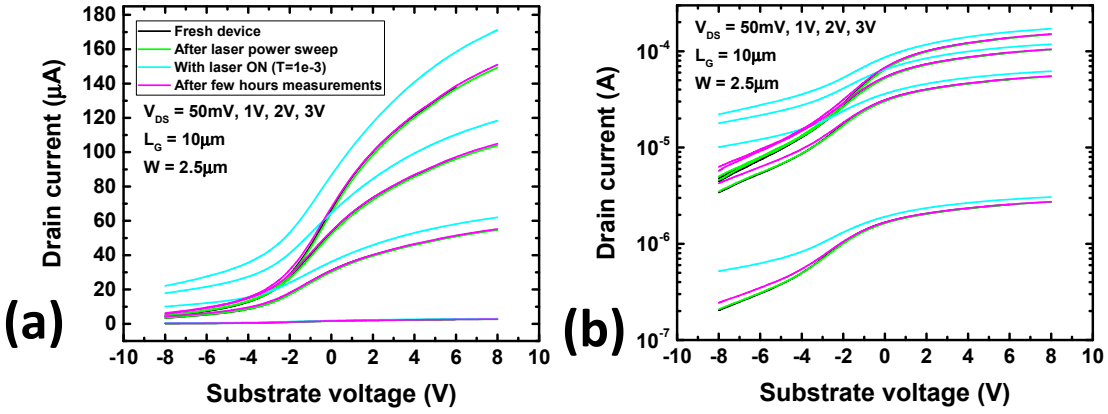

Figure 8: I_d-V_g characteristics measured for V_{ds} = 0.05, 0.5, 1, 2, and 3 V on fabricated ToF test structures featuring L_g = 10 µm, W=2.5 µm and t_{InGaAs} = 200 nm: (a) on a linear scale and (b) on a semi-log scale. Data are shown for the same device when measured for the first time (black), after having been subjected to a laser power sweep (see Fig. 9) (green), while being illuminated by the laser (blue), and after a few hours of measurements (pink).

In order to maximize the ToF signal for a minimized laser power, the thicker samples with a 200 nm thick InGaAs drift layer were used. Id-Vg transfer characteristics of the same ToF device with 10 µm gate length and 2.5 µm width are presented in Fig. 8 at various stage during the sample characterization in order to evaluate the stability of the sample. Compared to Fig. 7 and as expected, the I_{ON}/I_{OFF} ratio is reduced to a bit more than one order of magnitude as a result of the thicker InGaAs layer. Comparing the transfer characteristics of

the device in the dark (no laser illumination) when measured for the first time and after several hours of measurements being exposed to the laser, no change in on-current and threshold voltage can be observed, while off-current gets slightly degraded. We can conclude that the sample stability is sufficient to perform reproducible measurements.

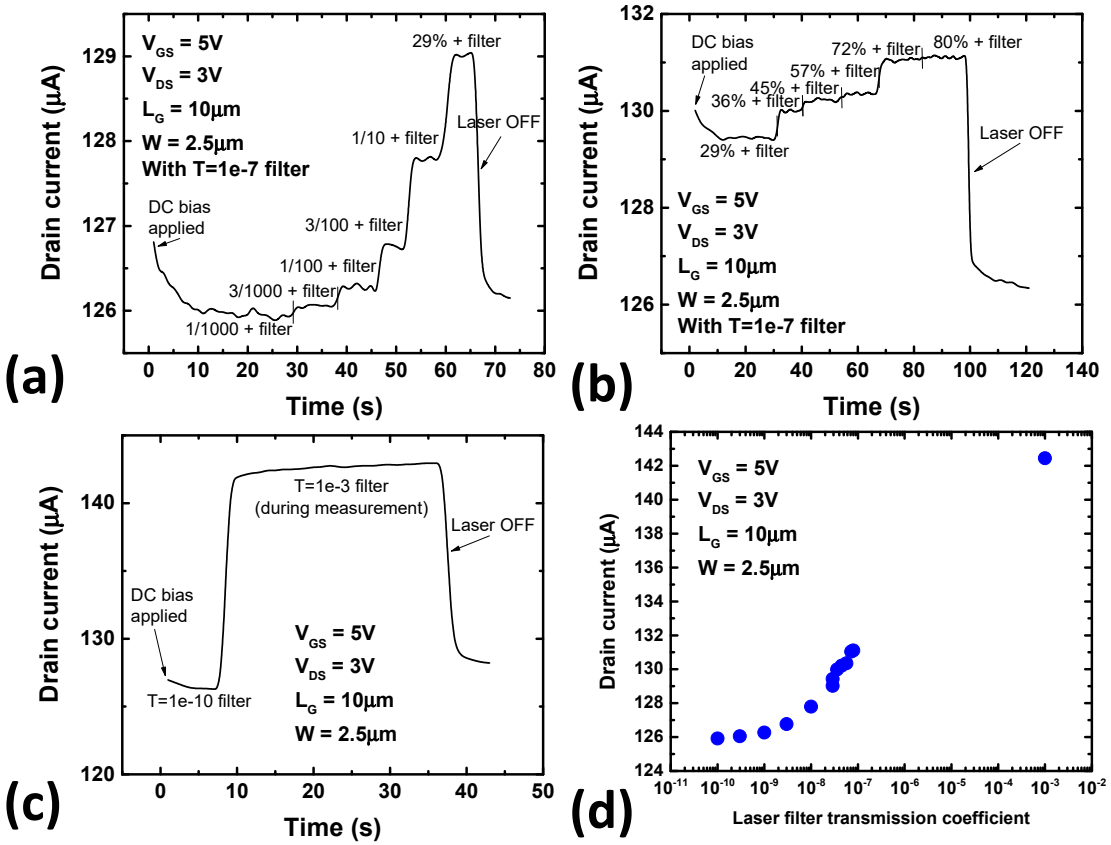

Figure 9: (a, b, c) Drain current versus time measured for V_{ds} = 3 V and V_{gs} = 5 V on fabricated ToF test structures featuring L_g = 10 µm, W=2.5 µm and t_{InGaAs} = 200 nm, while the transmission coefficient of the laser attenuators is being changed: (a) with the $T=10^{-7}$ filter while varying the tunable filter from 10^{-3} to 0.3, (b) with the $T=10^{-7}$ filter while varying the tunable filter from 0.3 to 0.8, (c) during a ToF measurement with the laser ON and attenuation filter of 10^{-3}. (d) Drain current versus laser filter transmission coefficient.

Comparing the transfer characteristics in the dark and under illumination of the laser attenuated with a transmission coefficient of 10^{-3}, a large increase in the on-current and off-current can be observed.

In order to understand the impact of the laser power on the DC characteristics, tunable filters are used to vary the laser power while the drain current is being recorded (Fig. 9). As explained in section 1.3, the average laser power is 150 mW, a tunable filter can be varied from a transmission coefficient of 10^{-3} to 1 and an ON/OFF filter can be inserted with a transmission coefficient of 10^{-7}. When the DC bias is applied to the sample, a transient phase where the drain current slowly decreases is observed for about 10 seconds (Fig. 9(a,b,c)). From this point, the tunable laser filtered is varied progressively while the ON/OFF filter is ON (Fig. 9(a,b)). A large increase of the drain current is observed with increasing transmission coefficients above 10^{-9} (above ≈0.15 nW average, ≈18 µW pulse assuming 100 fs pulse every 12 ns). Fig. 9(c) shows the drain current versus time during a ToF measurement with a filter transmission coefficient of 10^{-3}, showing an increase of the drain current from about 126 µA to 142 µA, for a laser power of ≈0.15 mW average, ≈18 W (!) pulse assuming 100 fs pulse every 12 ns. These results are summarized in Fig. 9(d) where the drain current is reported versus the filter transmission coefficient varied between 10^{-10} and 10^{-7}, with an extra point at 10^{-3} with the ON/OFF filter removed and the tunable filter to its maximum attenuation (≈0.15 mW average power). This last point corresponds to the minimum transmission coefficient giving enough signal on the scope to measure the transient response on the device under test and was used for all ToF measurements reported in the subsequent figures. It appears clearly that as the laser power is varied over 7 orders of magnitude, the average drain current is increasing by about 15%.

The time-resolved transient drain current acquired during the measurements shown in Fig. 9(c) is reported in Fig. 10(a), for two positions of the laser: at the drain contact edge and at the source contact edge. The transient current is reported after amplification by the 4-stage low-noise amplifier. It's absolute value is difficult to evaluate since the real transient current from the device might be attenuated by the impedance matching of the circuit, and the gain of the low-noise amplifiers depends on the frequency of the signal.

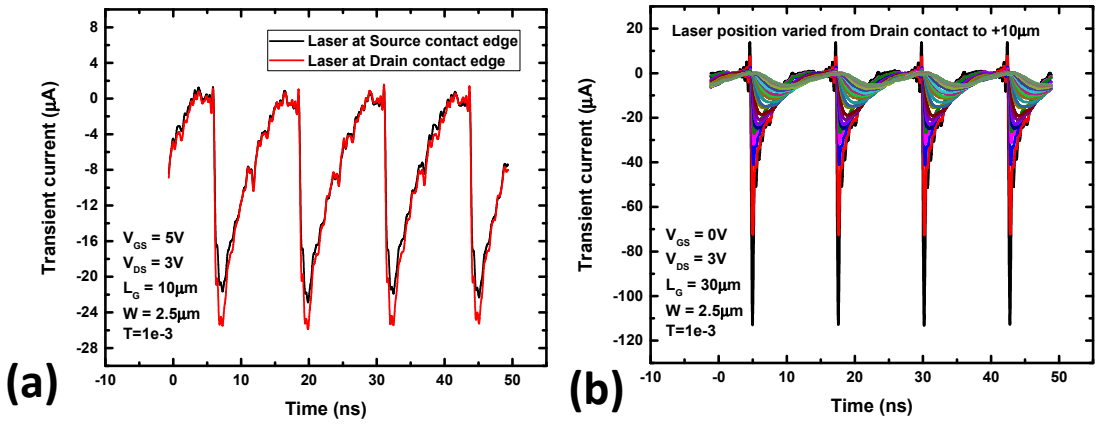

Figure 10: (a) Transient current versus time acquired at V_{ds} = 3 V and V_{gs} = 5 V on a ToF device featuring L_g = 10 µm, W=2.5 µm and t_{InGaAs} = 200 nm, with a laser filter transmission coefficient of 10^{-3}., the laser being aligned either on the source contact edge or the drain contact edge. These data were acquired at the same time as Fig. 9(c). The transient current is reported after amplification by the 4-stage low-noise amplifier. (b) Transient current versus time acquired at V_{ds} = 3 V and V_{gs} = 0 V on a ToF device featuring L_g = 30 µm, W=2.5 µm and t_{InGaAs} = 200 nm, with a laser filter transmission coefficient of 10^{-3}., the laser position being varied from the drain contact edge to +10 µm. The transient current is reported after amplification by the 4-stage low-noise amplifier.

Although a transient current signal is clearly detected, its line shape is not as expected from a typical ToF measurement (see Fig. 1(c)): it strongly decays versus time instead of being constant during the carrier transit time. Furthermore, the line shape of the signal is almost identical when the laser is aligned to the source or drain contact edge, while this should change the type of carriers drifting across the sample and hence the time constants.

In a typical ToF experiment, if the laser is positioned in the center of the sample rather than next to a contact, the expected line shape should present two plateaus: a first one whose amplitude corresponds to the drift current of electrons and holes for a time equal to the transit time of electrons (since they are expected to be faster), then a second plateau of lower amplitude corresponding only to the drift current of holes until the transit time of holes

is reached. Figure 10(b) presents the time-resolved transient current of a 30 µm long ToF device as the laser is moved from the drain contact edge to about +10 µm along the InGaAs drift layer. It appears clearly that the signal is vanishing and its time constant is increased as the laser is moved away from the contact edge, unlike the expected behaviour explained above for a typical ToF experiment. It appears that the generated electron-hole pairs have difficulties to reach the contact either because they are captured by traps or because the density of generated electron-hole pairs is so high that 1) carrier to carrier repulsion broadens the drifting carrier cloud, or 2) the field created by the electron-hole plasma completely screens the externally applied electric field which prevents electron-hole pairs from being separated (Canali, 2005) and are therefore likely to recombine radiatively. This second hypothesis seems likely given the laser power used for this measurement and its large impact on the DC current (Fig. 9(c)), which is the minimum laser power achievable in this setup to detect a time-resolved signal.

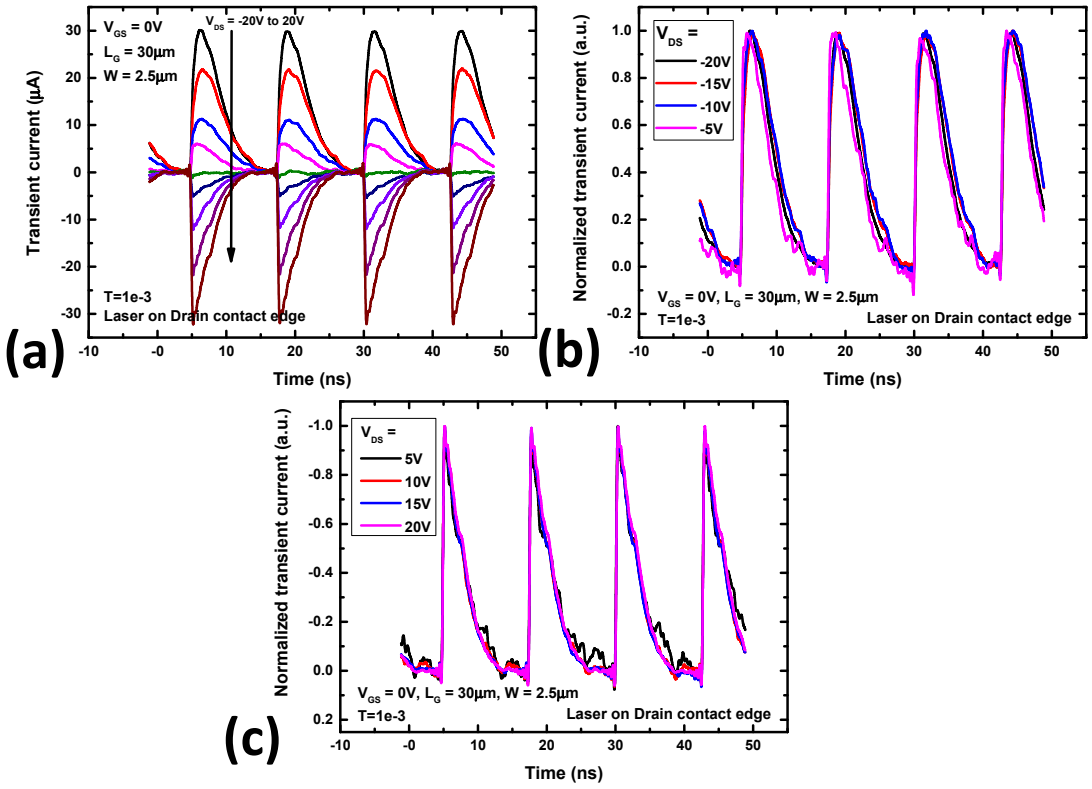

Figure 11: (a) Transient current versus time acquired at V_{ds} = 3 V and V_{gs} = 0 V on a ToF device featuring L_g = 30 µm, W=2.5 µm and t_{InGaAs} = 200 nm, with a laser filter transmission coefficient of 10^{-3}., the laser being aligned on the drain contact edge. The transient current is reported after amplification by the 4-stage low-noise amplifier. (b, c) Normalized transient current from Fig. 11(a) for (b) positive and (c) negative drain bias.

In order to study the influence of the applied lateral electric field, time-resolved transient drain current was measured on a 30 µm long ToF device as a function of the applied drain bias varied from -20V to +20V (+/- 6.7 kV/cm), with the laser aligned on the drain contact edge. The data are reported in Fig. 11(a), transient current is shown after amplification by the 4-stage low-noise amplifier. Changing the sign of the applied bias is expected to change the type of carriers drifting across the sample in a typical ToF experiment. In this case, it appears that varying the bias mostly impacts the amplitude and sign of the signal, but for a given

polarity, a varied bias does not seem to affect the line shape of the signal. This is confirmed in Fig. 11(b, c) by plotting the normalized transient current for a varying negative (Fig. 11(b)) or positive (Fig. 11(c)) bias: all normalized time-resolved drain current curves are almost exactly falling on top of each other. It shows that the applied bias is not influencing the dynamic response of the device. This evidence seems to confirm that the high density of electron-hole pairs creates its own internal electric field which screens the externally applied electric field.

As the results presented in Fig. 10(b) suggest that the time constant of the transient drain current depends on the position of the laser, another set of time-resolved transient drain current was acquired on the same 30 µm long ToF device as a function of the applied drain bias varied from -20V to +20V (+/- 6.7 kV/cm), with the laser aligned on the drain contact edge and then moved about 3.5 µm away from the contact along the InGaAs drift layer (Fig. 12(a)). As expected from previous results, the amplitude of the signal drops and the time constant (defined as the time width at 50% of the maximum amplitude) at positive drain bias increases from 3.2 ns to 4.5 ns. Comparing the normalized time-resolved drain currents at different drain bias (Fig 12(b,c)) reveals that again, the time constants do not depend on the externally applied electric field.

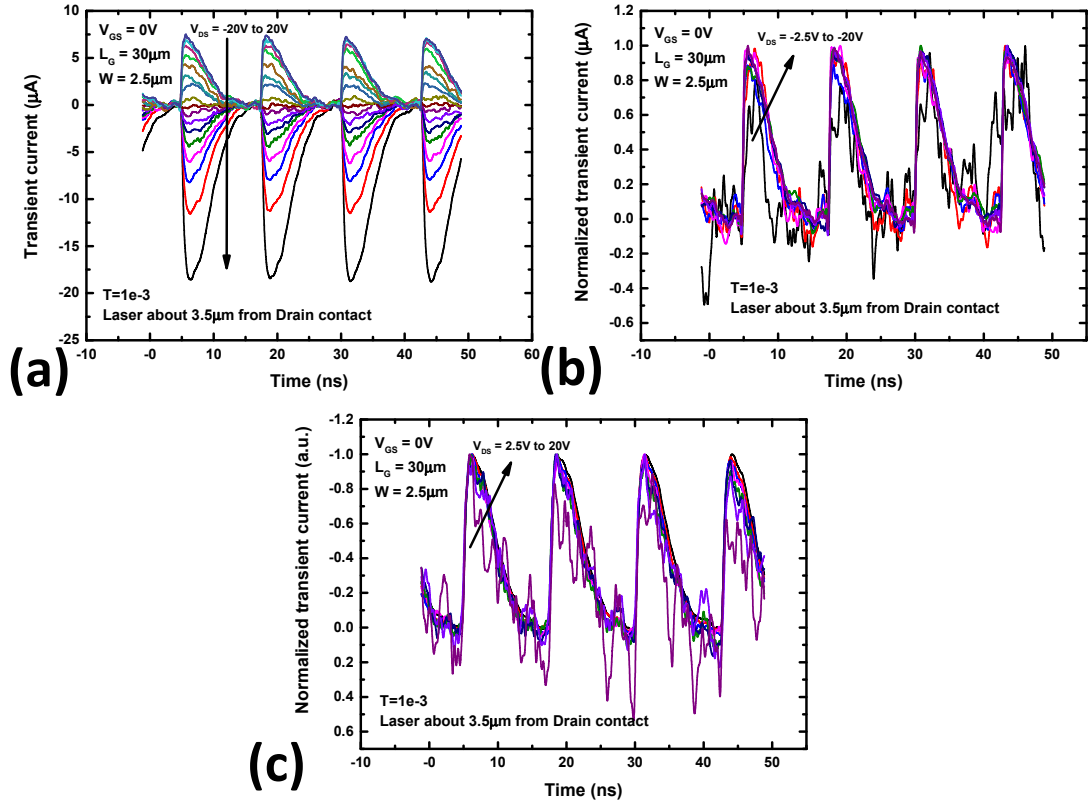

Figure 12: (a) Transient current versus time acquired at V_{ds} = 3 V and V_{gs} = 0 V on a ToF device featuring L_g = 30 µm, W=2.5 µm and t_{InGaAs} = 200 nm, with a laser filter transmission coefficient of 10^{-3}., the laser being aligned on the drain contact edge and then moved by about 3.5 µm away from the contact, along the InGaAs drift layer. The transient current is reported after amplification by the 4-stage low-noise amplifier. (b, c) Normalized transient current from Fig. 11(a) for (b) positive and (c) negative drain bias.

All those results seem to indicate that the minimum required laser power to have a measurable time-resolved signal is too large and that the proper conditions to perform a ToF measurements cannot be satisfied in this configuration. A new method is required to keep the same level of transient current (so that it can be detected) but lowering the laser power to levels where the generated electron-hole pairs would only represent a small perturbation of the charge in the device. It can be achieved by increasing the width of the ToF devices. On

the mask, ToF device width was varied from 2.5 μm to 25 μm – which is too small to give enough signal at low laser power. The rationale was that the laser has to be very well focused to a few microns to ensure that the length over which electron-hole pairs are generated is small compared to the drift length (see section 1.2). Therefore, a point focus was chosen to reach about 2 μm spot size and wide ToF devices (above 5 μm) cannot be homogeneously irradiated by the laser along the contact edge. If ToF devices would have a width W of few millimetres (which would be the correct size to have enough transient current but very low laser power), the laser would have to be focused in the form of a very long (milimeters) and narrow (few microns) line, perfectly aligned with the contact edge all along the sample. It can be achieved by the use of a Powell lens which can provide a long and narrow line with a uniform power density distribution. An attempt was made to realize such experiment. It was found that in order to have a laser line width as small as few microns, the geometry was such that it was not possible to physically fit an imaging objective and the RF picoprobe to contact the sample. A completely new setup would have to be re-designed, new masks and new wafers would have to be fabricated which was beyond the scope of the project.

In typical ToF experiments, the sample is “bulk”-like and illuminated from the top with a collimated laser beam of a few milimeters in diameter which gives a very large signal as carriers are traveling vertically through the sample, even with small laser power. The requirement of a small spatial distribution of the generated electron-hole pairs is given by the short absorption length (few microns) of the laser when it penetrates the sample surface, giving full freedom to shape the laser on the surface as desired to maximize the signal. In our lateral ToF configuration, the shape of the laser beam determines the distribution of electron-hole pairs in the drift direction and the sample thickness is fixed, which leaves only one degree of freedom to maximize the signal making the experiment extremely difficult.

Conclusions & Outlook

The time-of-flight method was described in order to characterize the drift velocity of carriers versus an externally applied electric field.

Dedicated time-of-flight (ToF) devices were designed, fabricated and characterized to study transport in InGaAs-on-insulator samples.

A dedicated experimental setup was designed and built comprising: a piezo-controlled 3-axis stage to position the sample, a parameter analyser to bias the device, an RF circuit to collect and amplify the time-resolved signal, a fast oscilloscope to acquire the time-resolved signal, a femtosecond laser to illuminate the sample, an optical bench to shape and position the laser and image the sample, and a fast photodiode to synchronize the laser with the electronics.

ToF devices were successfully characterized for their DC and time-resolved transient response under illumination of the pulsed laser as a function of the applied bias, laser position and laser power.

The results indicates that the required laser power to measure a sufficient time resolved transient current signal is too high, such that the cloud of electron-hole pairs has a too high density and its internally created electric field screens the externally applied electric field. Therefore, carriers are not separated and drifting through the sample as expected in a ToF experiment. The acquired data has nevertheless been delivered to the modelling partners to study the dynamics of the generation-recombination transients in these devices, and its relation to the density of interface and border traps, which are known to hamper the performance of state-of-the-art III-V MOSFETs.

After examination of recent literature, which does not report any result on this subject, ToF measures retain their relevance for the study of high field transport in thin III-V semiconductor films. However, it is foreseen that a successful completion of these experiments in thin films and with the available lasers would require a redesign of the setup and the fabrication of devices with new layouts, hence, significant new resources.

As regards the originally conceived use of the ToF data for calibration of velocity-field characteristics in thin III-V semiconductor films, a backup strategy has been implemented based on curves calculated with the most advanced high-level tools developed within the project. These results will be shown in future deliverables and reports.

References

Canali, C. (2005). Drift Velocity and Diffusion Coefficients from Time-of-Flight Measurements. In L. Reggiani, *Hot-Electron Transport in Semiconductors* (pp. 87-112). Vol 58 of Topics in Applied Physics.

Appendix

The test structure layer parameters (layer stack, thickness and doping etc.) detailed below are the same as in D3.4.

Table 1: Thickness and doping concentration of various layers in fabricated test structures.

Layer	Notation	Thickness Value(s)	Doping concentration
Si substrate	Si	525±25 µm	$2x10^{17}$ cm^{-3}, p type
BOX	t_{box}	25 nm SiO_2/10 nm Al_2O_3	
High-K interface layer (bottom)	t_{HK}	0.5 nm Al2O3/2 nm HfO2	
InGaAs	t_{InGaAs}	25, 50, 100 and 200 nm	$1\text{-}2x10^{16}$ cm^{-3}, n type
N+ RSD (InGaAs)	t_{rsd}	50 nm	$\sim5x10^{19}$ cm^{-3}, n type
High-K interface layer (top)	t_{HK}	0.5 nm Al_2O_3/2 nm HfO_2	